



Look beyond the status flow
The Attune™ NXT Flow Cytometer

Find out more

ThermoFisher
SCIENTIFIC



Protective T Cell Responses Featured by Concordant Recognition of Middle East Respiratory Syndrome Coronavirus–Derived CD8⁺ T Cell Epitopes and Host MHC

This information is current as of December 1, 2016.

William J. Liu, Jiaming Lan, Kefang Liu, Yao Deng, Yanfeng Yao, Shaolian Wu, Hong Chen, Lingling Bao, Haifeng Zhang, Min Zhao, Qihui Wang, Lingxia Han, Yan Chai, Jianxun Qi, Jincun Zhao, Songdong Meng, Chuan Qin, George F. Gao and Wenjie Tan

J Immunol published online 30 November 2016
<http://www.jimmunol.org/content/early/2016/11/29/jimmunol.1601542>

-
- Supplementary Material** <http://www.jimmunol.org/content/suppl/2016/11/29/jimmunol.1601542.DCSupplemental.html>
- Subscriptions** Information about subscribing to *The Journal of Immunology* is online at: <http://jimmunol.org/subscriptions>
- Permissions** Submit copyright permission requests at: <http://www.aai.org/ji/copyright.html>
- Email Alerts** Receive free email-alerts when new articles cite this article. Sign up at: <http://jimmunol.org/cgi/alerts/etoc>

The Journal of Immunology is published twice each month by
The American Association of Immunologists, Inc.,
9650 Rockville Pike, Bethesda, MD 20814-3994.
Copyright © 2016 by The American Association of
Immunologists, Inc. All rights reserved.
Print ISSN: 0022-1767 Online ISSN: 1550-6606.



Protective T Cell Responses Featured by Concordant Recognition of Middle East Respiratory Syndrome Coronavirus–Derived CD8⁺ T Cell Epitopes and Host MHC

William J. Liu,^{*,†,1} Jiaming Lan,^{†,‡,1} Kefang Liu,^{*,†,1} Yao Deng,^{†,1} Yanfeng Yao,^{§,1} Shaolian Wu,[¶] Hong Chen,[†] Lingling Bao,[§] Haifeng Zhang,^{*} Min Zhao,^{||} Qihui Wang,^{||} Lingxia Han,[¶] Yan Chai,^{||} Jianxun Qi,^{||} Jincun Zhao,[#] Songdong Meng,^{||} Chuan Qin,[§] George F. Gao,^{*,†,||,**} and Wenjie Tan^{*,†}

The coordinated recognition of virus-derived T cell epitopes and MHC molecules by T cells plays a pivotal role in cellular immunity–mediated virus clearance. It has been demonstrated that the conformation of MHC class I (MHC I) molecules can be adjusted by the presented peptide, which impacts T cell activation. However, it is still largely unknown whether the conformational shift of MHC I influences the protective effect of virus-specific T cells. In this study, utilizing the Middle East respiratory syndrome coronavirus–infected mouse model, we observed that through the unusual secondary anchor Ile5, a CD8⁺ T cell epitope drove the conformational fit of Trp⁷³ on the α 1 helix of murine MHC I H-2K^d. In vitro renaturation and circular dichroism assays indicated that this shift of the structure did not influence the peptide/MHC I binding affinity. Nevertheless, the T cell recognition and the protective effect of the peptide diminished when we made an Ile to Ala mutation at position 5 of the original peptide. The molecular bases of the concordant recognition of T cell epitopes and host MHC-dependent protection were demonstrated through both crystal structure determination and tetramer staining using the peptide–MHC complex. Our results indicate a coordinated MHC I/peptide interaction mechanism and provide a beneficial reference for T cell–oriented vaccine development against emerging viruses such as Middle East respiratory syndrome coronavirus. *The Journal of Immunology*, 2017, 198: 000–000.

Activation of T cells by the MHC/peptide complex may occur in three correlated ways: 1) direct interaction of the TCR with the MHC, termed MHC restriction; 2) direct interaction of the TCR with solvent-accessible peptide main chain and side chains; and 3) indirect interaction of peptide with TCR mediated via conformational perturbations in the MHC complex (1, 2). Crystallographic studies clearly showed that substitutions occurring at the peptides not only impact the exposed structure of the peptides, but they also lead to the induced fit on the helices of MHC that form the peptide-binding groove (3). This differential

tuning of the dynamic properties of MHC molecules by the peptides thus may impact TCR recognition (4). Furthermore, the binding peptide–affected portions on MHC protein comprise not only the regions contacted by TCRs but also other activating and inhibitory receptors of the immune system, such as the CD8 coreceptor and NK receptors (5). However, it is still largely unknown whether the conformational shift of MHC class I (MHC I) impacts the protection of Ag-specific T cells against specific virus infection.

In mid-2012, a novel coronavirus termed Middle East respiratory syndrome coronavirus (MERS-CoV) originated in Middle Eastern

^{*}College of Laboratory Medicine and Life Sciences, Institute of Medical Virology, Wenzhou Medical University, Wenzhou 325035, China; [†]Key Laboratory of Medical Virology, Ministry of Health, National Institute for Viral Disease Control and Prevention, Chinese Center for Disease Control and Prevention, Beijing 102206, China; [‡]Department of Pathogenic Biology, Hebei Medical University, Shijiazhuang 050017, China; [§]Institute of Laboratory Animal Sciences, Chinese Academy of Medical Sciences and Comparative Medicine Center, Peking Union Medical College, Key Laboratory of Human Disease Comparative Medicine, Ministry of Health, Beijing 100021, China; [¶]State Key Laboratory of Veterinary Biotechnology, Harbin Veterinary Research Institute, Chinese Academy of Agricultural Sciences, Harbin 150001, China; ^{||}CAS Key Laboratory of Pathogenic Microbiology and Immunology, Institute of Microbiology, Chinese Academy of Sciences, Beijing 100101, China; [#]State Key Laboratory of Respiratory Diseases, Guangzhou Institute of Respiratory Disease, First Affiliated Hospital of Guangzhou Medical University, Guangzhou 510120, China; and ^{**}Research Network of Immunity and Health, Beijing Institutes of Life Science, Chinese Academy of Sciences, Beijing 100101, China

¹W.J.L., J.L., K.L., Y.D., and Y.Y. contributed equally to this work.

ORCID: 0000-0002-5325-4077 (H.Z.); 0000-0002-1912-3620 (Y.C.).

Received for publication September 7, 2016. Accepted for publication November 6, 2016.

This work was supported by China Ministry of Science and Technology National 973 Project Grant 2015CB910500, National Key Plan for Scientific Research and Development of China Grants 2016YFD0500301, 2016YFD0500304, and 2016YFD0500305, National Natural Science Foundation of China Grants 81373141, 81401312, and 81461168030, Municipal Healthcare Joint Innovation Major Project of Guangzhou Grant 201604020011, and Megaproject for Infectious Disease Research of China

Grants 2016ZX10004222-003, 2014ZX10004001-002, 2014ZX10004001-006, and 2012ZX10004501-004. J.Z. is supported by the Thousand Talents Plan Award of China 2015. G.F.G. is a leading principal investigator of the National Natural Science Foundation of China Innovative Research Group (Grant 81321063).

Structure factors for MHC class I complexes H-2K^d/37-1, H-2K^d/37-3, H-2K^d/142-2, H-2K^d/142-5, and H-2K^d/15A presented in this article have been submitted to the Protein Data Bank (<http://www.rcsb.org>) under accession numbers 5GR7, 5GSB, 5GSX, 5GSV, and 5GSR, respectively.

The funders had no role in the study design, data collection and analysis, decision to publish, or preparation of the manuscript.

Address correspondence and reprint requests to Prof. George F. Gao or Dr. Wenjie Tan, Key Laboratory of Medical Virology, Ministry of Health, National Institute for Viral Disease Control and Prevention, Chinese Center for Disease Control and Prevention, 155 Changbai Road, Changping District, Beijing 102206, China (G.F.G.) or College of Laboratory Medicine and Life Sciences, Institute of Medical Virology, Wenzhou Medical University, Wenzhou 325035, China (W.T.). E-mail addresses: gaofu@chinaacdc.cn (G.F.G) or tanwj28@163.com (W.T.)

The online version of this article contains supplemental material.

Abbreviations used in this article: CD, circular dichroism; β_2m , β_2 -microglobulin; MERS, Middle East respiratory syndrome; MERS-CoV, Middle East respiratory syndrome coronavirus; MHC I, MHC class I; PDB, Protein Data Bank; SARS-CoV, severe acute respiratory syndrome coronavirus; SFC, spot-forming cell; S protein, spike protein; T_m , midpoint transition temperature.

Copyright © 2016 by The American Association of Immunologists, Inc. 0022-1767/16/\$30.00

countries. Later, imported cases were reported in countries from other continents (6–8), including South Korea and China in 2015 (9–11). The limited clues of adaptive immunity against MERS-CoV infection revealed that in patients infected with MERS-CoV, weak and delayed Ab responses are associated with more severe disease or fatal outcomes (12–14). However, recent evidence indicates that the neutralizing Ab levels in MERS patients are weakly and inversely correlated with the viral loads in the lower respiratory tract (13). This may indicate that the presence of Abs does not lead to the elimination of the virus from the lower respiratory tract. For the MERS-CoV-specific T cell responses, PBMCs obtained on day 24 of illness show a strong, specific T cell response against MERS-CoV spike protein (S protein) (15). Lymphocyte counts rapidly increased up to 10 d after symptom onset in MERS patients with or without mild pneumonia, whereas all of the deceased patients displayed rapid drops in their lymphocyte counts, suggesting that adaptive immune responses play a protective role (14). However, the molecular basis of MERS-CoV-specific T cell recognition during virus infection is still largely known.

Thus far, MERS-CoV vaccines have provided efficacious protection in animal models (16), although none of the vaccines has been applied in human clinical trials. Major strategies for vaccine development focus on the elicitation of immunity against the major Ag (S protein) of MERS-CoV (17, 18). Vaccination with recombinant receptor-binding domain protein induces robust Abs, alleviates pneumonia, and decreases viral load in monkeys (19). However, studies also demonstrate that MERS-CoV S protein-derived vaccines induce specific CD8⁺ T cell and virus-neutralizing Abs, which can contribute to complete protection against MERS-CoV in animal models (20, 21). Our recently developed MERS vaccines using an adenoviral-based encoded S protein induce strong neutralizing Abs and T cell immune responses, protecting immunized mice from challenge with MERS-CoV (22). However, knowledge is still limited concerning the T cell-mediated immunity of MERS-CoV among mice, which could be a useful research model for MERS-CoV vaccine development.

In this study, we evaluated the T cell immunogenicity of MERS-CoV S protein in a mouse model by using the overlapping peptides spanning the whole S protein. The MERS-CoV-derived T cell peptide possesses a feature to induce MHC fitting that has a pivotal impact on the immunogenicity of the peptide and its protective efficacy against MERS-CoV infection. These data demonstrate that T cells play a crucial but featured role in MERS-CoV clearance and may illuminate new avenues for vaccine development.

Materials and Methods

Mice

Six- to eight-week-old female BALB/c mice were purchased from the Animal Care Center of the Chinese Academy of Medical Science (Beijing, China) and maintained under specific pathogen-free conditions. All experiments were performed in strict compliance with the *Guide for the Care and Use of Laboratory Animals of the People's Republic of China*, and approved by the Committee on the Ethics of Animal Experiments of the Chinese Center for Disease Control and Prevention.

Animal immunization with MERS-CoV S protein vaccines

To evaluate the T cell immunogenicity of the MERS-CoV S protein, BALB/c mice were i.m. immunized with rAd5-S, an adenoviral-based S protein vaccine constructed in our laboratory (22), at a dosage of 5×10^9 virus particles. Two weeks later, the mice were sacrificed to harvest spleens.

For the antigenic comparison of peptide 37-1 and its substitution 15A, BALB/c mice were immunized through a prime/boost strategy. The cDNA pCAGGS-S vaccine expressing the S protein of MERS-CoV was used to immunize the mice, followed by a boost through a vaccinia vector vaccine rVV-Sq carrying the ectodomain of S protein. The T cell immune responses were detected 2 wk after the last injection.

Peptide immunization and MERS-CoV challenge

During the animal immunization with the Ag peptide, the mice were randomly divided into three groups. The mice in the control groups were immunized with adjuvants of 100 μ l of IFA and 10 μ g of murine heat shock protein gp96 (23). The mice in the other two groups were immunized with 10 μ g of peptide or variant peptide combined with the adjuvants. The mice were immunized twice with a 2-wk interval. Nine days after the last immunization, all of the mice were lightly euthanized with isoflurane and intranasally transduced with 2.5×10^8 PFU of Ad5-hDPP4 for the rapid generation of a mouse model of MERS-CoV infection (24). Five days later, the transduced mice were intranasally infected with MERS-CoV (1×10^5 PFU) in a total volume of 50 μ l of DMEM medium. Three days after infection by MERS-CoV, the mice were euthanized. Lung and trachea were harvested for pathological examination and virus isolation detection. The immunization and detection schedule is shown in Fig. 6A.

Peptide pool design and synthesis

Peptide pools spanning the entire S protein consisted of 161 short peptides that were coded from 1 to 161. They were synthesized by Beijing SciLight Biotechnology. Each peptide was an 18-mer and overlapped by 10 aa with its adjacent peptides. Three matrix peptide pools spanning the entire MERS-CoV S protein were designed for the detection of immunodominant T cell regions (Supplemental Table I). The subsequently defined short immunogenic CD8⁺ T cell epitopes were also synthesized as listed in Table I.

ELISPOT assays

To detect MERS-CoV-specific T cell responses, an IFN- γ ELISPOT assay was performed as described previously (20). Briefly, 96-well plates were coated with 100 μ l/well of 5 mg/ml anti-mouse IFN- γ Ab (BD Pharmingen, San Diego, CA) overnight at 4°C and then blocked for 2 h at room temperature. Mouse splenocytes, freshly isolated as described previously (25), were added to the plate (5×10^7 /well). Then, the matrix peptide pools (2 μ g/ml individual peptide) were added to the wells in duplicate. PMA and ionomycin were added to the positive control group, whereas the negative control group received no stimuli. After an 18-h incubation, a biotinylated detection Ab (BD Pharmingen) and streptavidin-HRP were added. Spots were developed by the addition of a 3-amino-9-ethylcarbazole substrate solution, which produced a colored spot after a 5- to 30-min incubation in the dark at room temperature. Finally, IFN- γ spot-forming cells (SFCs) were counted through an ELISPOT reader.

Intracellular cytokine staining

The intracellular cytokine staining assays were conducted as previously described (26). Briefly, splenocytes (2.5×10^6 per sample) were cultured for 4 h at 37°C in 96-well round-bottom microtiter plates with complete RPMI 1640 culture supplemented with peptide at a concentration of 4 μ g/ml. Control cells were incubated with an unrelated peptide or without peptide. Brefeldin A was then added and incubated with the cells for 2 h before staining. The cells were next incubated for 30 min at 4°C with 50 μ l of a 1:100 dilution of an FITC-labeled Ab targeting mouse CD8 and PerCP-labeled anti-CD4. Subsequently, the cells were permeabilized in Cytofix/Cytoperm for 20 min at 4°C, washed three times with Perm/Wash buffer, and incubated in the same buffer for 30 min at 4°C with 50 μ l of a 1:100 dilution of allophycocyanin-labeled Ab targeting mouse IFN- γ . The results were then detected using a FACSCalibur flow cytometer (BD Biosciences). The above reagents and Abs were purchased from BD Pharmingen.

H&E staining

Histopathological examinations were conducted as previously described (19). Briefly, lungs and trachea were collected after the mice were euthanized. Procedures were performed using samples fixed in 10% neutral buffered formalin, embedded in paraffin, sequentially sectioned to 4 μ m thickness, and stained with H&E prior to examination by light microscopy.

Virus isolation

The MERS-CoV isolation was conducted on Vero cells. Briefly, the lungs were homogenized to a final 10% suspension in DMEM and clarified by low-speed centrifugation at $4500 \times g$ for 30 min at 4°C. Vero cells (1.5×10^4 /well) were seeded in 96-well plates and incubated overnight at 37°C in a CO₂ incubator. One hundred microliters of 10-fold serially diluted suspension was then added to each well in quadruplicate. The virus was allowed to adsorb onto the cells at 37°C for 1 h. After adsorption, viral inoculates were removed, and 100 μ l of DMEM (2% FBS) was added to each well. Plates were incubated in a CO₂ incubator at 37°C for 3 d, following which cytopathic effects were microscopically observed at $\times 40$ magnification.

Refolding and purification of H-2K^d

Murine MHC I H-2K^d H chain and human β_2 -microglobulin (β_2m) were overexpressed as inclusion bodies in the BL21(DE3) strain of *Escherichia coli*. Renaturation and purification of H-2K^d assembled with immunodominant peptides were performed as described previously (27). Generally, injection and dilution of MHC H chain, β_2m , and peptide occurred at a molar ratio of 1:1:3 in an L-arginine refolding buffer. After 24 h for protein refolding, the H-2K^d complexes were concentrated and exchanged into a buffer of 20 mM Tris-HCl (pH 8) and 50 mM NaCl and then purified using Superdex 200 10/300 GL gel filtration chromatography (GE Healthcare, Beijing, China).

Tetramer preparation and cell staining

H-2K^d-restricted tetramers of peptides 37-1, I5A (37-1 variant), and mutant H-2K^d (named W73A-restricted tetramers of peptide 37-1) were prepared as previously described (28). Briefly, to produce biotinylated peptide/MHC protein, H-2K^d was modified by the addition of a substrate sequence for the biotinylating enzyme BirA at the C terminus of the $\alpha 3$ domain. In vitro-renatured H-2K^d-peptide complexes were then purified and biotinylated by incubation with D-biotin, ATP, and the biotin protein ligase BirA (Avidity) at 4°C for 12 h. The biotinylated H-2K^d was further purified over a Superdex 200 10/300 GL gel filtration column (GE Healthcare) to remove excess biotin and then mixed with PE-streptavidin (Sigma-Aldrich). Cells from the subjects were stained with PE-tetramer and FITC-conjugated anti-CD8 Ab. All samples were analyzed with a FACSCalibur flow cytometer (BD Biosciences) after staining.

Generation of specific T cell lines in vitro

Splenocytes from immunized mice were incubated with peptides in RPMI 1640 containing 10% FBS (HyClone Laboratories) at 37°C with 5% CO₂ at a density of 2.5×10^6 cells/ml in 24-well plates. On day 2, 50 U/ml recombinant mouse IL-2 was added to the medium. Half of the medium was exchanged with supplementation by recombinant mouse IL-2 on days 4 and 7. On day 9, cells were harvested and tested for the presence of MERS-CoV-specific CD8⁺ T cells by tetramer staining.

Thermostability measurements using circular dichroism

To evaluate the thermostability of H-2K^d complexes formed with different peptides, we used the circular dichroism (CD) spectroscopy method as previously described (29). All complexes were prepared as described above and diluted to 200 μ g/ml in 20 mM Tris-HCl (pH 8) and 50 mM NaCl. CD spectra at 218 nm were measured on a Chirascan spectrometer (Applied Photophysics) using a thermostatically controlled cuvette at temperature intervals of 0.1°C and a rate of 1°C/min between 20 and 100°C. The proportion of denatured protein was calculated from the mean residue ellipticity (u) using the standard method: fraction unfolded (%) = $(\theta - \theta_N)/(\theta_U - \theta_N)$, where θ_N and θ_U are the mean residue ellipticity values in the fully folded and fully unfolded states, respectively. The midpoint transition temperature (T_m) was calculated using the data from the denaturation curves in the program Origin 8.0 (OriginLab).

X-ray crystallography, structure determination, and refinement

The refolded H2-K^d/peptide complexes were further purified through a Resource Q ion exchange column (GE Healthcare), and the concentration of the complexes was adjusted to 5–15 mg/ml. As described previously (30), crystals were grown by the hanging drop vapor diffusion method at 18°C. The H2-K^d/peptide complex was screened through Crystal Screen kit I/II, the Index Screen kit, and the PEGRx kit (Hampton Research). For cryoprotection, crystals were transferred to reservoir solutions containing 20% glycerol and then flash cooled and maintained at 100 K in a cryostream. X-ray diffraction data were collected at beamline BL17U of the Shanghai Synchrotron Radiation Facility. The structures were determined using molecular replacement with the program CNS (31). The model used was the structure coordinates with Protein Data Bank (PDB) code 1VGK. Extensive model building was performed by hand using COOT (32), and restrained refinement was performed using REFMAC5 (33). The stereochemical quality of the final model was assessed with the program PROCHECK (34). Structure-related figures were generated using PyMOL (<http://www.pymol.org/>).

Statistical analysis

The null hypothesis proposed that tested parameters in different immunized mouse groups would not differ significantly from each other. Differences in mean values were evaluated for statistical significance ($p < 0.05$ or < 0.01) by a Student two-tailed *t* test. Data were assembled and statistically calculated on computerized spreadsheet programs (Excel [Microsoft] and Prism 5 [GraphPad Software]).

Protein structure accession numbers

The coordinates and structure factors of complexes H-2K^d/37-1, H-2K^d/37-3, H-2K^d/142-2, H-2K^d/142-5, and H-2K^d/I5A were deposited in the PDB under accession numbers 5GR7, 5GSB, 5GSX, 5GSV, and 5GSR, respectively.

Results

Immunodominant regions in the MERS-CoV S protein

A detailed immunogenic mapping analysis of the peptides spanning the entire S protein was conducted in mice immunized with the adenoviral-based S protein-encoding vaccine rAd5-S. By crossing the 12 immunogenic matrix peptide pools (Fig. 1A, 1B) inducing high levels of IFN- γ secretion (≥ 200 SFCs/ 10^6 splenocytes), eight different immunodominant peptide regions covering 18 aa were identified in S protein, including five regions in the N-terminal domain, one in the receptor-binding domain, and two in the S2 domain of S protein (Fig. 1D).

To acquire the shortest immunogenic H2-K^d-restricted CD8⁺ T cell epitopes of the three immunodominant peptides 37, 122, and 142 (≥ 600 SFCs/ 10^6 splenocytes), the peptides were truncated into short fragments (Table I). ELISPOT assays were performed to evaluate the T cell responses to these shortened peptides with typical H-2K^d-binding peptide motifs (Y/F at P2 position and L/I/V at Pc position). Within all the truncated smaller fragments, the peptides 37-1, 37-3, 122-1, 122-3, 142-2, and 142-5 resulted in almost as high a level of T cell responses as for the original peptides (Fig. 1C, 1D).

Structure-based determination of epitope clusters in S protein

The 9-mer peptide 37-1 and 10-mer peptide 142-2 are the C-terminal truncations of the longer peptides 37-3 and 142-5, respectively. To determine whether 37-3 and 142-5 were independent epitopes or whether their immunogenicities depended on the shorter peptides 37-1 and 142-2, we determined the molecular structures of all four peptides complexed with H2-K^d (Table II). The overall complex structures of H2-K^d with peptides 37-1 (Fig. 2A), 37-3 (Fig. 2B), 142-2 (Fig. 2C), and 142-5 (Fig. 2D) are similar to other MHC I molecules, with the peptides lying on the bed formed by two α helices and β -sheets in the $\alpha 1\alpha 2$ domain of H-2K^d. Peptide 37-1 is presented in the groove of H-2K^d, with the P2-Tyr and P9-Ile as the primary anchoring residues in pockets B and F, respectively (Fig. 2A). Similarly, peptide 142-2 has Tyr² and Leu¹⁰ as its primary anchors (Fig. 2C). Interestingly, peptides 37-3 and 142-5 assume similar conformations as the truncated 37-1 and 142-2 peptides, respectively. No electron densities were observed for the N-terminal residue P1-Lys for 37-3 or N-terminal residue P1-Ser for 142-5. This may indicate that the immunogenicities of peptides 37-3 and 142-5 depend on the shorter peptides 37-1 and 142-2.

Structural shift of H-2K^d impelled by MERS-CoV peptide

When comparing the two structures of H-2K^d complexed with peptides 37-1 and 142-2, we found that Trp⁷³ in the α helix of H-2K^d had different conformations. In the structure of H-2K^d/142-2 (Fig. 3A), Trp⁷³ is located under the C-terminal portion of the peptide, which leads to a C-terminal bulged conformation for 142-2 as common H-2K^d-presented peptides. In the H-2K^d/37-1 complex (Fig. 3B), however, Trp⁷³ protrudes out of the H-2K^d peptide-binding groove, being solvent exposed and ready for TCR recognition. We compared the Trp⁷³ of H-2K^d/37-1 with the corresponding residue in all previously determined complexes of H-2K^d with T cell epitopes derived from HBV (PDB code 1VGK), influenza virus (2FWO), insulin (4WDI), and glucose-6-phosphatase catalytic subunit-related protein (3NWM) (35–37). We found that Trp⁷³ from all of the previously determined structures of H-2K^d is pointing

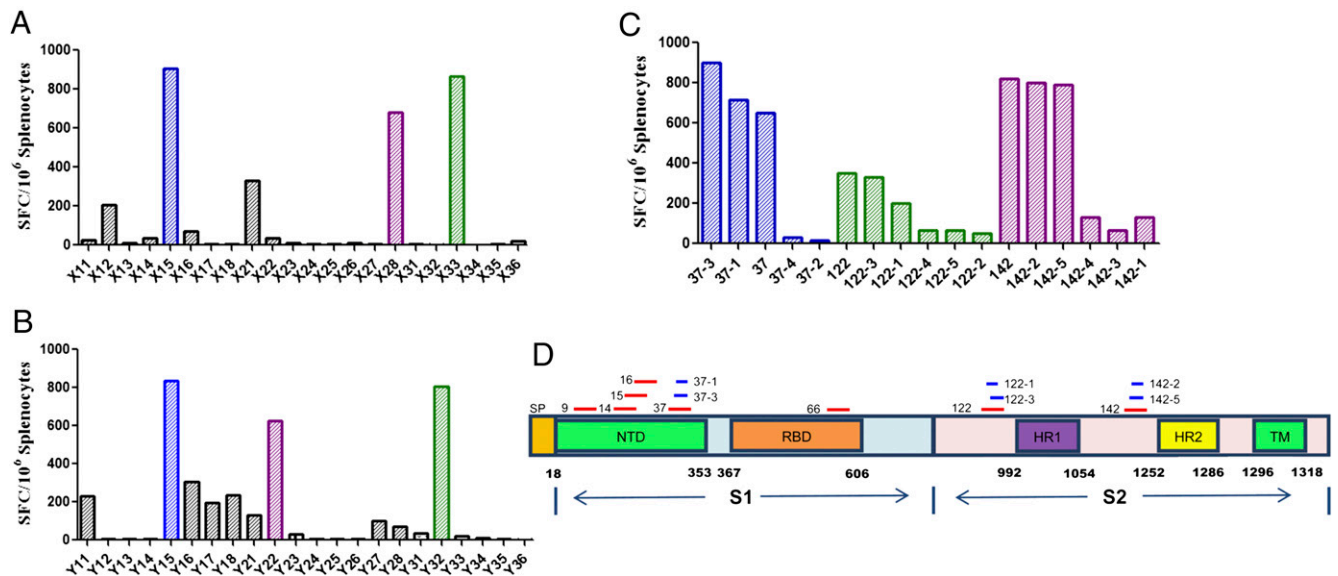


FIGURE 1. Systematic evaluation of immunodominant regions within the MERS-CoV S protein. Overlapping peptides covering the entire S protein of MERS-CoV were synthesized (Supplemental Table I). **(A and B)** Matrix peptide pools were mixed with different combinations of the peptides to map immunodominant regions. The cutoff for the T cell responses of the peptide pools was denoted as red dashed lines. Six immunogenic peptide-comprising pools that induce high levels of IFN- γ secretion (≥ 600 SFCs/ 10^6 splenocytes) are highlighted by colored columns. Peptide 37 (blue) was identified by the cross of pools X15 and Y15. Similarly, the immunogenic peptides 122 (purple) and 142 (green) were defined by X28/Y22 and X33/Y32, respectively. **(C)** Different peptide truncations were synthesized (shown in Table II) to identify the short immunogenic CD8⁺ T cell epitopes within peptides 37, 122, and 142. The T cell responses of the shortened peptides were evaluated by ELISPOT assays using freshly isolated splenocytes from MERS-CoV S protein vaccine-immunized mice. **(D)** The schematic structure of S protein shows the distribution of cellular immunodominant regions. Eight immunodominant regions were displayed as red lines, and the well-defined short CD8⁺ T cell epitopes were shown as blue lines. HR1/2, heptad repeat 1/2; NTD, N-terminal domain; RBD, receptor-binding domain; SP, signal peptide; TM, transmembrane domain.

into the groove under the peptides (Fig. 3E), similar to Trp⁷³ in the H-2K^d/142-2 structure. Only the Trp⁷³ of H-2K^d/37-1 protrudes out of the groove. Further analysis of the structures indicated that the secondary anchor P5-Ile in the middle of peptide 37-1 contributes to the conformational shift of H-2K^d Trp⁷³. P5-Ile in peptide 37-1 is larger than the corresponding secondary anchors of other peptides in H-2K^d complexes. The steric hindrance of peptide 37-1 P5-Ile with the Trp⁷³ of H-2K^d pushes Trp⁷³ out of the peptide-binding groove. Furthermore, the main chain position of

peptide 37-1 is lower in the groove and closer to $\alpha 1$ helix when compared with all other peptides presented by H-2K^d (Fig. 3C, 3D).

Immunogenicity of MERS-CoV peptide affected by peptide/MHC I interaction

The uncommon upward protrusion of Trp⁷³ in the H-2K^d structure with peptide 37-1 implies that the T cell recognition of 37-1 may depend on both the unique conformation of the peptide and H-2K^d itself. To verify this hypothesis, we immunized BALB/c mice with

Table I. Peptide information

Peptide	Position	Sequence	Binding Score (BIMAS) ^a
37	S(289–306)	TIKYYSIIPHRSIRSIQSD	— ^b
37-1	S(292–300)	<u>YYSIIPHSI</u> ^c	2400.0
37-2	S(291–299)	KYYSIIPHS	86.4
37-3	S(289–300)	<u>KYYSIIPHSI</u>	3456.0
37-4	S(292–299)	YYSIIPHS	80.0
15A	S(292–300)	YYSI <u>A</u> PHSI ^d	2000.0
122	S(969–986)	AIPFAQSIFYRLNGVGIT	—
122-1	S(972–980)	<u>FAQSIFYRL</u>	69.1
122-2	S(977–985)	FYRLNGVGI	2400.0
122-3	S(977–986)	<u>FYRLNGVGIT</u>	60.0
122-4	S(976–983)	SFYAPEPI	240.0
122-5	S(976–986)	SFYAPEPITSL	960.0
142	S(1187–1204)	TGSSFYAPEPITSLNTKY	—
142-1	S(1191–1199)	FYAPEPITS	60.0
142-2	S(1191–1200)	<u>FYAPEPITSL</u>	2880.0
142-3	S(1190–1198)	SFYAPEPIT	24.0
142-4	S(1190–1197)	SFYAPEPI	960.0
142-5	S(1190–1200)	<u>SFYAPEPITSL</u>	—

^aEstimated half-time of dissociation of H-2K^d peptide complexes calculated using the BIMAS program (http://bimas.dcert.nih.gov/molbio/hla_bind/index.html).

^bEstimated half-time of dissociation of peptide >10 is not available.

^cThe antigenic peptides in Fig. 1D are underlined.

^dThe mutated residue I>A is underlined.

Table II. X-ray data processing and refinement statistics

Parameter	H-2K ^d /37-1	H-2K ^d /37-3	H-2K ^d /142-2	H-2K ^d /142-5	H-2K ^d /I5A
PDB code	5GR7	5GSB	5GSX	5GSV	5GSR
Data processing					
Space group	P2 ₁ 2 ₁ 2 ₁	P2 ₁ 2 ₁ 2 ₁	C2	P2	P2 ₁
Cell parameters (Å)	<i>a</i> = 50.0 <i>b</i> = 74.6 <i>c</i> = 121.1 α = 90.0 β = 90.0 γ = 90.0	<i>a</i> = 50.2 <i>b</i> = 76.0 <i>c</i> = 122.3 α = 90.0 β = 90.0 γ = 90.0	<i>a</i> = 102.6 <i>b</i> = 68.5 <i>c</i> = 145.1 α = 90.0 β = 106.8 γ = 90.0	<i>a</i> = 57.5 <i>b</i> = 45.9 <i>c</i> = 71.6 α = 90.0 β = 108.7 γ = 90.0	<i>a</i> = 50.353 <i>b</i> = 79.658 <i>c</i> = 122.706 α = 90.0 β = 90.3 γ = 90.0
Wavelength (Å)	1.54178	1.00000	1.54178	0.97915	0.97944
Resolution (Å)	50.0–2.4(2.49–2.40) ^a	50.0–1.8(1.86–1.80)	50.0–2.5(2.59–2.50)	50–2.0(2.07–2.0)	50–2.2(2.28–2.2)
Total reflections	168,813	274,523	123,285	131,573	230,665
Completeness (%)	97.4 (86.3)	98.9 (97.9)	93.6 (92.3)	96.8 (96.8)	98.2 (94.3)
<i>R</i> _{merge} (%) ^b	9 (36.8)	7.2 (36.8)	8.5 (53.4)	15.2 (125.2)	6.6 (27.3)
<i>I</i> / σ	24.7 (4.3)	20.0 (5.7)	15.0 (2.3)	1.5 (1.5)	20.5 (5.7)
Refinement					
<i>R</i> _{factor} (%) ^c	20.1	19.3	19.5	20.0	20.3
<i>R</i> _{free} (%)	25.7	22.2	24.2	25.2	23.1
r.m.s.d.					
Bonds (Å)	0.003	0.008	0.006	0.004	0.007
Angles (°)	0.696	1.171	1.083	0.911	0.773
Ramachandran map					
Most favored (%)	90.4	91.0	90.9	89.2	96.2
Additional allowed (%)	9.0	7.8	7.9	9.9	3.8
Generously allowed (%)	0.6	1.2	1.2	0.6	0.4
Disallowed (%)	0	0.0	0.0	0.3	0.0

^aValues in parentheses refer to statistics in the outermost resolution shell.

^b $R_{\text{merge}} = \sum_{hkl} \sum_i |I_i - \langle I \rangle| / \sum_{hkl} \sum_i I_i$, where I_i is the observed intensity and $\langle I \rangle$ is the average intensity of multiple observations of symmetry-related reflections.

^c $R = \sum_{hkl} |F_{\text{obs}}| - k|F_{\text{calc}}| / \sum_{hkl} |F_{\text{obs}}|$, where R_{free} is calculated for a randomly chosen 5% of reflections, and R_{work} is calculated for the remaining 95% of reflections used for structure refinement.

r.m.s.d., root mean square deviation.

the cDNA pCAGGS-S vaccine expressing the S protein of MERS-CoV and boosted immunization through the vaccinia vector-based vaccine rVV-Sq. A robust T cell response against peptides 37 (1316 ± 31 SFCs/10⁵ splenocytes) and 37-1 (1181 ± 102 SFCs/10⁵ splenocytes) was detected (Fig. 4A). However, we detected a much lower T cell response (761 ± 105 SFCs/10⁵ splenocytes) to the mutant peptide I5A containing a substitution at position 5 of 37-1 from Ile to Ala. The decreased antigenicity of I5A compared with 37-1 was also confirmed through intracellular cytokine staining assays (Fig. 4B) (1.19% IFN⁺CD8⁺ T cells for I5A versus 2.91% IFN⁺CD8⁺ T cells for 37-1). Meanwhile, we also detected MERS-CoV-specific T cell responses in the mouse group that was not booster immunized with rVV-Sq. An antigenic decrease of peptide I5A was still observed despite the low T cell responses in these mice (Fig. 4).

To clarify the mechanistic details of the impact of the peptide/H-2K^d interaction on T cell recognition, we prepared three different MHC tetramers for MERS-CoV-specific T cell detection: 1) H-2K^d with peptide 37-1, 2) H-2K^d with peptide I5A, and 3) an MHC tetramer W73A comprised of peptide 37-1 and mutant H-2K^d with a Trp⁷³Ala substitution. For the freshly isolated splenocytes from MERS-CoV vaccine-immunized mice (Fig. 4C, 4D), 3.56% 37-1-specific CD8⁺ T cells were detected, much higher than the 0.102% from tetramer prepared with wild-type H-2K^d and peptide I5A. The ratio of tetramer W73A-specific T cells was higher than that of I5A but still lower than the wild-type tetramer of the H-2K^d/37-1 complex.

We also established peptide-specific T cell lines by culturing the splenocytes from vaccinated mice under the stimulation of peptides 37-1 and I5A, respectively, to investigate the different immunogenicities of these two peptides. After in vitro stimulation by peptide 37-1 or I5A for 9 d, the 37-1 tetramer-specific CD8⁺ T cells accounted for 57.6 ± 10.3% among the 37-1-cultured cells, higher than the 36.4 ± 8.0% among the I5A-cultured splenocytes.

Thus, I5A had a lower ability to stimulate 37-1-specific T cells in vitro compared with wild-type peptide 37-1 (Fig. 4E, 4F).

To further demonstrate the molecular basis for the concordant T cell recognition of MERS-CoV-derived CD8⁺ T cell epitopes and host MHC I, we determined the binding affinity of mutant I5A to H-2K^d through in vitro refolding (Fig. 5A) and CD (Fig. 5B). We found that mutant I5 (46°C) has a similar binding affinity for H-2K^d as does peptide 37-1 (45°C), with comparable *T_{ms}*. This indicated that substitution from Ile⁵ to Ala⁵ in peptide 37-1 does not influence the peptide-binding affinity to H-2K^d. Instead, the major antigenic variance of I5A compared with 37-1 may be contributed by conformational shifts in both the peptide and H-2K^d itself. To verify this hypothesis, we determined the x-ray crystal structure of H-2K^d complexed to the 37-1 mutant I5A. As expected based on our hypothesis, the Trp⁷³ in H-2K^d/I5A was lower into the groove due to sufficient space left by the P5-Ala of peptide I5A (Fig. 5C). The main chain conformation of peptide I5A also shifts back to the traditional C-terminal bulged position (Fig. 5D). The position of I5A is higher than 37-1, especially the His⁷ of I5A, which is boosted by Trp⁷³ from beneath.

Based on the structures of H-2K^d complexed with 37-1 and I5A, we deduced that our W73A tetramer (with wild-type peptide 37-1 and the H-2K^d Trp⁷³Ala mutant) had an intermediate structure between H-2K^d/37-1 and H-2K^d/I5A. In the W73A tetramer, the conformation of peptide 37-1 would remain the same as in the structure of H-2K^d/37-1, and the mutation of Trp to Ala at position 73 of H-2K^d would be the only difference from the wild type. Thus, the tetramer W73A-specific T cells had an intermediate ratio, higher than that of H-2K^d/I5A and lower than the wild-type tetramer of H-2K^d/37-1.

The MHC conformation-concordant protective effect of peptide 37-1

To investigate the protective effect of peptide 37-1 against MERS-CoV infection and its molecular basis, we used our previously

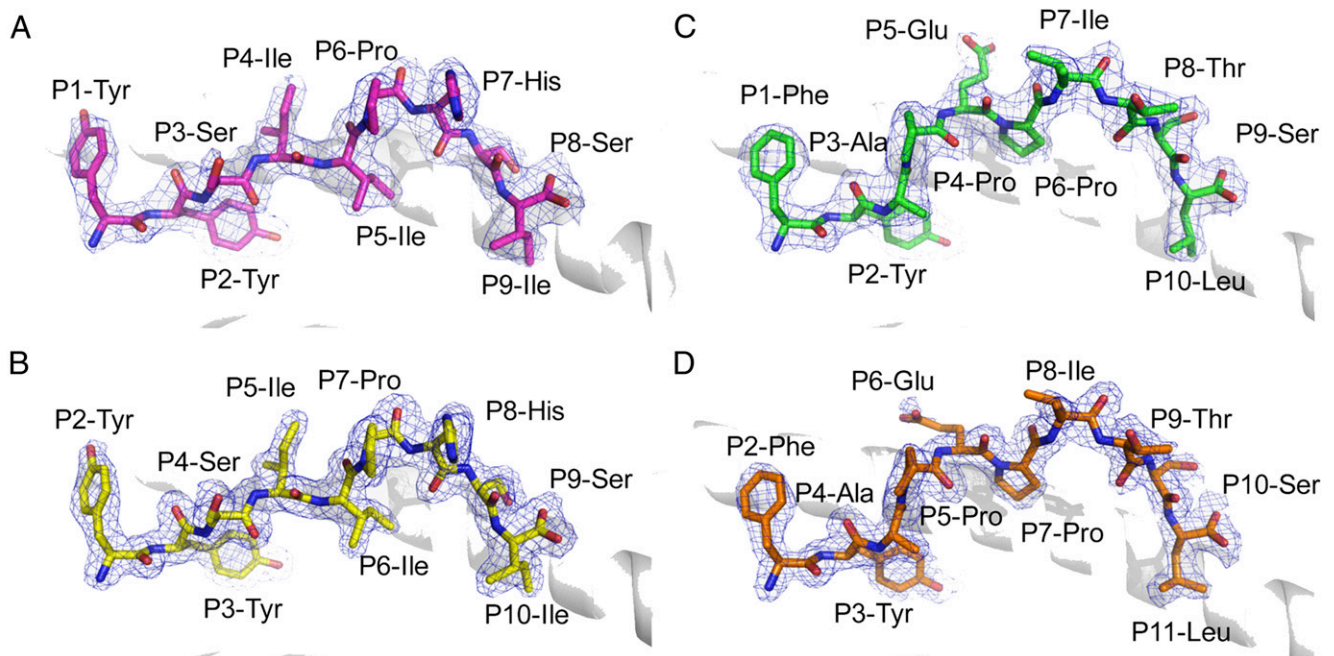


FIGURE 2. Structure-based definition of short antigenic CD8⁺ T cell epitopes. (**A** and **B**) Conformations of peptides 37-1 (**A**) and 37-3 (**B**) in the groove of H-2K^d are displayed through the *2Fo-Fc* electron density maps contoured at 1.0 σ . The electron densities are shown as blue mesh viewed in profile with the α 2 helix removed for clarity. (**C** and **D**) The *2Fo-Fc* electron density maps of peptides 142-2 and 142-5 presented by H-2K^d. No electron densities were observed for the N-terminal residue P1-Lys for 37-3 or N-terminal residue P1-Ser for 142-5.

established mouse model of MERS-CoV infection (Fig. 6A) (24). The mice immunized with peptide 37-1 had a quicker body weight recovery after MERS-CoV challenge compared with the adjuvant IFA/Gp97-immunized mouse group, although without a significant

difference (Fig. 6B). The virus titers of the 37-1 group were much lower than those of the adjuvant group on day 3 after virus challenge, indicating quick virus clearance by 37-1-specific T cells (Fig. 6C). The histopathological examinations of lungs and trachea in the

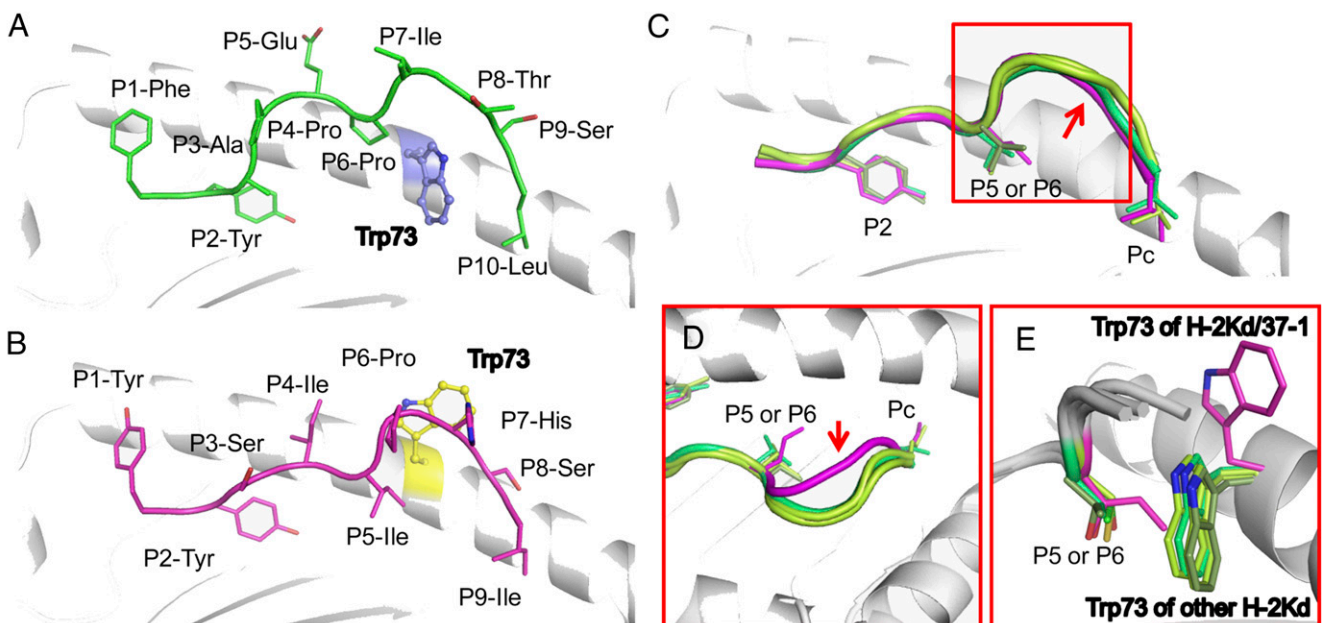


FIGURE 3. Unique conformation of H-2K^d when bound to 37-1. (**A**) In the structure of H-2K^d/142-2, the Trp⁷³ (green) of H-2K^d protrudes into the groove. The Pro⁶ of peptide 142-2 acts as the secondary anchor in the M-shaped conformation of the peptide. (**B**) The main chain of peptide 37-1 is shown as a purple loop with the side chains as purple sticks. P5-Ile of peptide 37-1 acts as a secondary anchoring residue in the middle portion of the peptide. Trp⁷³ of H-2K^d, shown in purple sticks and spheres, displays an upward conformation. (**C**) The superimposition of peptide 37-1 (purple loop) with the peptides (different shades of green) from all of the previously determined H-2K^d structures (1VGK, 2FWO, 3NWM, and 4WDI). Only the side chains of anchoring residues are shown herein in sticks. The lower position of the 37-1 main chain is indicated by a red arrow. The details in the red square are shown in (**D**) and (**E**). (**D**) The upside view of the bulged C termini [red square in (**C**)] showing the conformational differences of peptide 37-1 (purple) with other peptides (shades of green) presented by H-2K^d. (**E**) The coordination of Trp⁷³ of H-2K^d with the peptides in the groove. The longer P5-Ile side chain of 37-1 results in steric hindrance with the Trp⁷³ in the structures of H-2K^d when binding to other peptides.

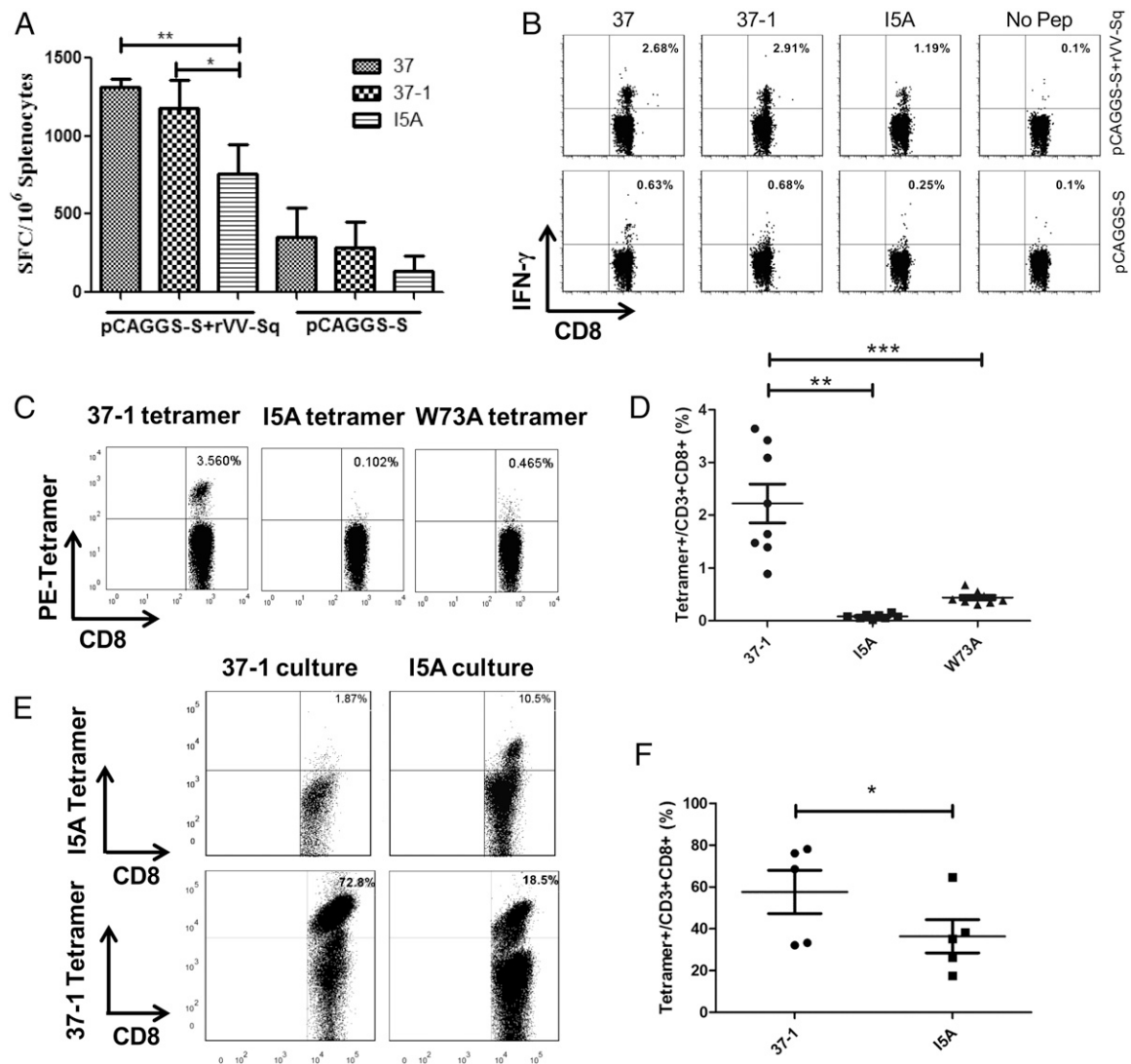


FIGURE 4. Conformation-dependent antigenicity of peptide 37-1. **(A)** The peptide 37-, 37-1-, and I5A (the mutant of 37-1 at position 5 from Ile to Ala)-specific T cell responses were detected through IFN- γ by using freshly isolated splenocytes from MERS-CoV vaccine-immunized mice. pCAGGS-S, BALB/c mice were immunized with cDNA pCAGGS-S vaccine expressing S protein only; pCAGGS-S+rVV-Sq, BALB/c mice were immunized through a prime of cDNA pCAGGS-S vaccine expressing S protein, followed by a vaccinia vector vaccine rVV-Sq carrying the ectodomain of S protein. **(B)** Intracellular cytokine staining was manipulated to detect the peptide-specific CD8⁺ T cells. Different peptides were used as stimulators to induce the secretion of IFN- γ before the test. The samples without peptide stimulation (No Pep) were used as negative controls. Lymphocytes were gated through the side light scatter/forward light scatter parameters. CD8⁺ T cells were subsequently selected for the secretion of IFN- γ . **(C)** The MERS-CoV-specific CD8⁺ T cells in the freshly isolated splenocytes from vaccinated mice were stained with tetramers 37-1 (complexes between H-2K^d and wild-type peptide 37-1), I5A (complexes between H-K^d and mutated peptide I5A), and W73A (complexes between the H-2K^d Trp⁷³Ala mutant and wild-type peptide 37-1). Lymphocytes were gated through the side light scatter/forward light scatter parameters. CD8⁺ T cells were subsequently selected for the analysis of tetramers. **(D)** Statistical analysis of the tetramer⁺ CD8⁺ T cells among total CD8⁺ T cells in (C). **(E)** The splenocytes from vaccinated mice were cultured in vitro for 9 d under the stimulation of peptide 37-1 and I5A, respectively. On day 9, the MERS-CoV-specific CD8⁺ T cell lines were analyzed by the staining of tetramers 37-1 and I5A. **(F)** Statistical analysis of the tetramer 37-1 staining of the T cell lines established by in vitro culturing using peptides 37-1 and I5A, respectively. * $p < 0.05$, ** $p < 0.01$, *** $p < 0.001$.

MERS-CoV-infected mice revealed that the inflammatory responses in both the bronchiole and alveolus were milder in 37-1-immunized mice than the adjuvant IFA/Gp97-immunized group (Fig. 6D).

No protective effect of the peptide I5A-specific T cell response against MERS-CoV was observed, as revealed by similar virus titers of the mice immunized with I5A and the adjuvant IFA/Gp97 (Fig. 6C). This indicates that the protective effect of peptide 37-1 depends on the unique structural orchestration of this MERS-CoV-derived peptide and the host MHC I itself.

Discussion

Four years have elapsed since the first MERS-CoV case was reported in the Middle East. However, studies on MERS-CoV-specific T cell

immunity and its protective effect are still ongoing. In this study, we evaluated the T cell immunodominance of the MERS-CoV S protein by using the overlapping peptides spanning the whole protein. A concordant recognition of MERS-CoV-derived novel CD8⁺ T cell epitopes and host MHC I by specific T cells was shown. Furthermore, the protective effect provided by the coordinated T cell responses and the molecular basis of this phenomenon were demonstrated. Our study sheds light on a new mechanism of virus-specific T cell recognition and may impact vaccine development for MERS-CoV.

Natural infection with severe acute respiratory syndrome coronavirus (SARS-CoV) and inoculation with related vaccines give rise to dominant responses against the structural Ags of SARS-CoV in

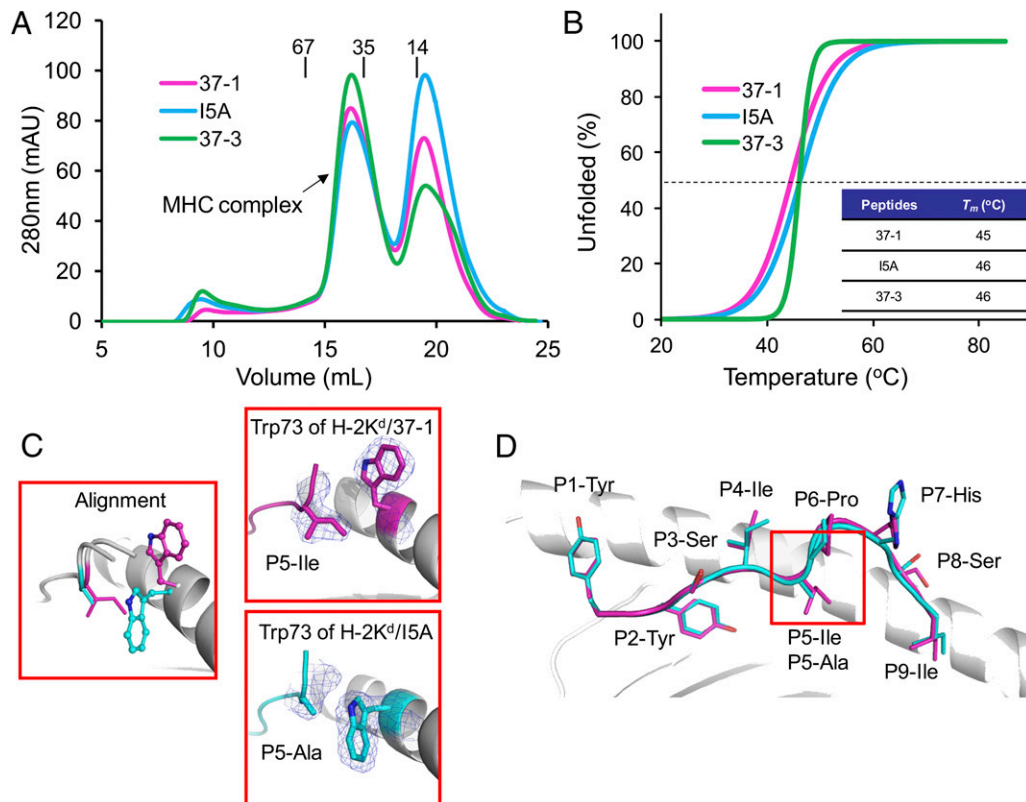


FIGURE 5. The conformational shift of H-2K^d depends on the Ile⁵ of peptide 37-1. **(A)** Binding of peptides 37-1 and I5A to H-2K^d were elucidated by in vitro refolding. Peptides with the ability to bind to H-2K^d help the H-2K^d H chain and murine β_2m to refold in vitro. After properly refolding, the high-absorbance peaks of the MHCs with the expected molecular mass of 45 kDa eluted at the estimated volume of 16 ml on a Superdex 200 10/300 GL column. The profile is marked with the approximate positions of the molecular mass standards of 67.0, 35.0, and 14.0 kDa. Complexes were formed by refolding peptides 37-1 and 37-3, indicating a comparable binding capability of the two peptides to H-2K^d. Soluble MHC I complexes were formed by renaturation, indicating a comparable binding capability of the peptides 37-1 and I5A to H-2K^d. **(B)** Thermostability of 37-1, 37-3, and mutant I5A/MHC complexes as revealed by CD spectroscopy. The T_m s of different peptides are indicated by the gray dashed line 50% fraction unfolded. **(C)** The conformation of W73 on the $\alpha 1$ helix of H-2K^d when bound to I5A is different from the Trp⁷³ in the H-2K^d/37-1 complex. The solid conformations of the Trp⁷³ in both structures are displayed through the *2Fo-Fc* electron density maps contoured at 1.0 σ . **(D)** Superimposition of peptide 37-1 (purple loops and sticks) with its mutant I5A (cyan loops and sticks). The position of the mutation is indicated by a red square.

humans and animals (38, 39). Xu and coworkers (40) detected SARS-CoV-specific T cell responses among PBMCs from donors who recovered from SARS using overlapping peptides covering the entire SARS-CoV proteome. They found that most of the antigenic peptides are located in the structural proteins (especially S protein) rather than in nonstructural proteins. Meanwhile, several HLA-A2-restricted CD8⁺ T cell-specific epitopes derived from the SARS-CoV S proteins have been identified (41–43). All of these data from SARS-CoV imply a crucial role of S protein as a T cell immunodominant Ag for coronaviruses. For MERS-CoV, several H-2^d- and H-2^b-restricted CD8⁺ T cell epitopes have recently been identified through an in vitro T cell epitope prediction strategy using the mouse model sensitized to MERS-CoV infection (24). In the present study, we evaluated the cellular immunodominant regions of the entire MERS-CoV S protein. Several previously identified CD8⁺ T cell epitopes (24) were included in the immunodominant regions we defined, which corroborates our studies. The identified cellular immunodominant regions of the S protein will be helpful for MERS-CoV-specific T cell studies using animal models and for the development of vaccines (44–46).

Previously, we defined a clustering region of CTL epitopes within the transmembrane region of the M protein (25, 47). The antigenic 9-mer peptide Md3-C9 (LACFVLA AV) is the C-terminal truncation of the 10-mer T cell epitope Md3 (TLACFVLA AV). The crystal structure of HLA-A*0201 complexed with peptide Md3

(PDB code 3I6K) shows that the peptide conformation is different from the structure of Md3-C9 (PDB code 3TO2) via the use of a distinct P2 anchor residue. This indicates that the antigenicity of Md3 is independent of its C-terminal truncation Md3-C9. In our current crystal structures of H-2K^d, the peptide conformation and the anchoring residues of the 10-mer peptide 37-3 and 11-mer peptide 142-5 are similar to their C terminal truncations, that is, the 9-mer peptide 37-1 and the 10-mer peptide 142-2, respectively. This indicates that the antigenicities of peptide 37-3 and 142-5 are dependent on the shorter peptides 37-1 and 142-2. The T cell repertoires of the peptides 37-3 and 142-5 may also largely overlap with peptides 37-1 and 142-2, with an eye to the commonly shared TCR repertoire by different but mimic peptides (48). In the structures, no electron densities for the P1-Lys of 37-3 or P1-Ser of 142-5 can be observed, perhaps due to the flexibility of these residues. Another possibility is that these residues may have been degraded during crystal growth. However, during the T cell responses in mice infected with MERS-CoV, 37-3 and 142-5 may still be naturally processed and presented by H-2K^d. Additionally, these peptides with residues protruding out of the N terminus of the peptide-binding groove may be recognized by specific TCRs and induce unique T cell repertoires that are different from the one of 37-1 and 142-2.

In the present study, the mice immunized with peptide 37-1 together with murine Gp96 protein had a lower virus titer and quicker body weight recovery after MERS-CoV infection. This

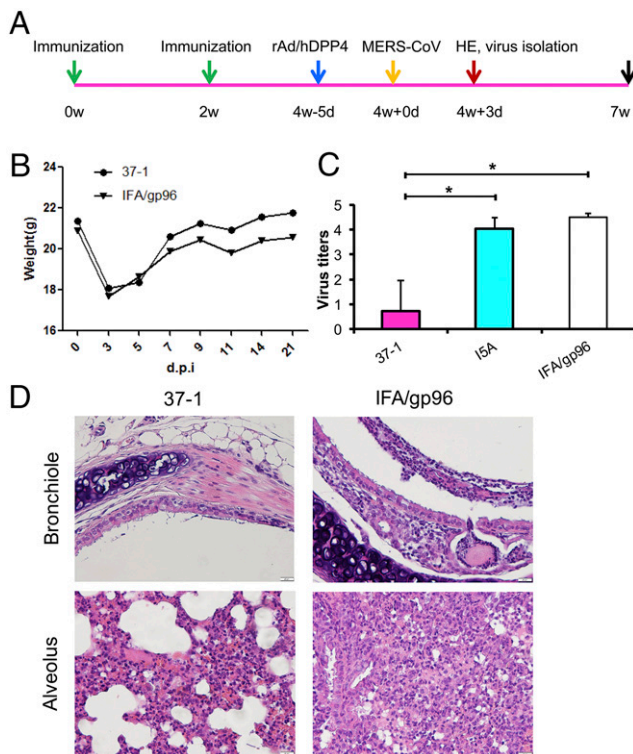


FIGURE 6. Conformation-dependent protection of 37-1-specific T cell immunity against MERS-CoV infection. **(A)** Flowchart of immunization, virus challenge, and virus detection in the mouse model. The time of immunization with peptide, IFA, and gp96 is shown as a green arrow. The time for intranasal transduction of Ad5-hDPP4 to rapidly generate a mouse model of MERS-CoV infection is denoted as a blue arrow. The time for infection with MERS-CoV is shown as an orange arrow. The time to euthanize the mice, assess pathology, and detect virus is shown as a brown arrow. The last day for the body weight measurement is denoted with a black arrow. **(B)** Body weight of the mice after MERS-CoV infection. Quicker weight recovery of the peptide 37-1-immunized group was observed compared with the adjuvant control. **(C)** Virus titers in the lungs of the mice 3 d after MERS-CoV infection. The mouse groups immunized with different peptides or PBS before virus infection are shown in different columns. $*p < 0.05$. **(D)** Histopathological examination of the lungs and trachea of the mice 3 d after MERS-CoV infection. Sections were stained with H&E. Original magnification, $\times 100$.

indicates the important role of T cells for anti-MERS-CoV vaccine development, comparable to the previous discovery on SARS-CoV peptide vaccines (44). However, no protective effect against MERS-CoV infection can be observed after the preemptive immunization of the mutated peptide I5A. This can be partially explained by the altered exposed surface of the peptide and the induced fit of Trp⁷³ of host MHC I. In previous studies on influenza virus-derived peptides and T cell immunity-escaping mutants, the engineered viruses with the mutated sites within T cell epitopes induced diminished CD8⁺ T cell responses and selected narrowed TCR repertoires (49, 50). This can be partially explained by the MHC/peptide structures that showed a loss of contacts between the peptides and His¹⁵⁵ of H-2D^b (50), or the altered topography of His¹⁵⁵ (49), a position known to play an important role in mediating TCR/MHC interactions. In our study, minimal MERS-CoV-specific T cells can be stained by the mutant I5A tetramer compared with the wild-type peptide 37-1 tetramer, which may also reflect a narrowed TCR repertoire corresponding to I5A.

It has been indicated that peptides impose subtle structural transitions on MHC molecules that affect T cell recognition and may thus be critical for virus clearance by T cell responses (49, 50).

Previously, we determined the structure of bovine MHC I N*01801 complexed with a rinderpest virus epitope, which shows two distinct conformations (51). A detailed analysis of the structure revealed that the polymorphic amino acid Ile⁷³ within the MHC groove has a propensity to adopt different conformations to accommodate the rinderpest virus peptide. Interestingly, in our present structure of H-2K^d/37-1, the Trp that displays an induced conformation is also at position 73. Thus, the polymorphic amino acid in position 73 of MHC I from different mammals may act as a key residue for the peptide/MHC I interaction, impacting the T cell recognition.

Our data provide a novel MHC I and peptide resonant interaction for subsequent protective T cell immunity and may aid in vaccine development for emerging infectious viruses such as MERS-CoV.

Acknowledgments

We thank Dr. Bart L. Haagmans and Dr. Ron A. M. Fouchier (Erasmus MC, Rotterdam, the Netherlands) for providing MERS-CoV (isolate hCoV-EMC/2012). We also thank Prof. Stanley Perlman (University of Iowa, Iowa City, IA) for providing the rAd5-hDPP4 stock. We are also grateful to Prof. Jianfang Zhou (National Institute for Viral Disease Control and Prevention, Chinese Center for Disease Control and Prevention) for excellent assistance on the flow cytometry.

Disclosures

The authors have no financial conflicts of interest.

References

- Baker, B. M., D. R. Scott, S. J. Blevins, and W. F. Hawse. 2012. Structural and dynamic control of T-cell receptor specificity, cross-reactivity, and binding mechanism. *Immunol. Rev.* 250: 10–31.
- Gras, S., S. R. Burrows, S. J. Turner, A. K. Sewell, J. McCluskey, and J. Rossjohn. 2012. A structural voyage toward an understanding of the MHC-I-restricted immune response: lessons learned and much to be learned. *Immunol. Rev.* 250: 61–81.
- Insaïdo, F. K., O. Y. Borbulevich, M. Hossain, S. M. Santhanagopalan, T. K. Baxter, and B. M. Baker. 2011. Loss of T cell antigen recognition arising from changes in peptide and major histocompatibility complex protein flexibility: implications for vaccine design. *J. Biol. Chem.* 286: 40163–40173.
- Borbulevich, O. Y., K. H. Piepenbrink, B. E. Gloor, D. R. Scott, R. F. Sommese, D. K. Cole, A. K. Sewell, and B. M. Baker. 2009. T cell receptor cross-reactivity directed by antigen-dependent tuning of peptide-MHC molecular flexibility. *Immunity* 31: 885–896.
- Hawse, W. F., B. E. Gloor, C. M. Ayres, K. Kho, E. Nuter, and B. M. Baker. 2013. Peptide modulation of class I major histocompatibility complex protein molecular flexibility and the implications for immune recognition. *J. Biol. Chem.* 288: 24372–24381.
- Geng, H., and W. Tan. 2013. A novel human coronavirus: Middle East respiratory syndrome human coronavirus. *Sci. China Life Sci.* 56: 683–687.
- Hijawi, B., M. Abdallat, A. Sayaydeh, S. Alqasrawi, A. Haddadin, N. Jaaroud, S. Alsheikh, and T. Alsanouri. 2013. Novel coronavirus infections in Jordan, April 2012: epidemiological findings from a retrospective investigation. *East. Mediterr. Health J.* 19(Suppl. 1): S12–S18.
- Zaki, A. M., S. van Boheemen, T. M. Bestebroer, A. D. Osterhaus, and R. A. Fouchier. 2012. Isolation of a novel coronavirus from a man with pneumonia in Saudi Arabia. *N. Engl. J. Med.* 367: 1814–1820.
- Su, S., G. Wong, Y. Liu, G. F. Gao, S. Li, and Y. Bi. 2015. MERS in South Korea and China: a potential outbreak threat? *Lancet* 385: 2349–2350.
- Wang, Y., D. Liu, W. Shi, R. Lu, W. Wang, Y. Zhao, Y. Deng, W. Zhou, H. Ren, J. Wu, et al. 2015. Origin and possible genetic recombination of the middle east respiratory syndrome coronavirus from the first imported case in China: phylogenetics and coalescence analysis. *MBio* 6: e01280–e15.
- Kim, J. I., Y. J. Kim, P. Lemey, I. Lee, S. Park, J. Y. Bae, D. Kim, H. Kim, S. I. Jang, J. S. Yang, et al. 2016. The recent ancestry of Middle East respiratory syndrome coronavirus in Korea has been shaped by recombination. *Sci. Rep.* 6: 18825.
- Park, W. B., R. A. Perera, P. G. Choe, E. H. Lau, S. J. Choi, J. Y. Chun, H. S. Oh, K. H. Song, J. H. Bang, E. S. Kim, et al. 2015. Kinetics of serologic responses to MERS coronavirus infection in humans, South Korea. *Emerg. Infect. Dis.* 21: 2186–2189.
- Corman, V. M., A. M. Albarak, A. S. Omrani, M. M. Albarak, M. E. Farah, M. Almasri, D. Muth, A. Sieberg, B. Meyer, A. M. Assiri, et al. 2016. Viral shedding and antibody response in 37 patients with Middle East respiratory syndrome coronavirus infection. *Clin. Infect. Dis.* 62: 477–483.
- Min, C. K., S. Cheon, N. Y. Ha, K. M. Sohn, Y. Kim, A. Aigerim, H. M. Shin, J. Y. Choi, K. S. Inn, J. H. Kim, et al. 2016. Comparative and kinetic analysis of viral shedding and immunological responses in MERS patients representing a broad spectrum of disease severity. *Sci. Rep.* 6: 25359.

15. Guan, W. D., C. K. Mok, Z. L. Chen, L. Q. Feng, Z. T. Li, J. C. Huang, C. W. Ke, X. Deng, Y. Ling, S. G. Wu, et al. 2015. Characteristics of traveler with Middle East respiratory syndrome, China, 2015. *Emerg. Infect. Dis.* 21: 2278–2280.
16. Du, L., W. Tai, Y. Zhou, and S. Jiang. 2016. Vaccines for the prevention against the threat of MERS-CoV. *Expert Rev. Vaccines* 15: 1123–1134.
17. Zhang, N., S. Jiang, and L. Du. 2014. Current advancements and potential strategies in the development of MERS-CoV vaccines. *Expert Rev. Vaccines* 13: 761–774.
18. Wang, Q., G. Wong, G. Lu, J. Yan, and G. F. Gao. 2016. MERS-CoV spike protein: targets for vaccines and therapeutics. *Antiviral Res.* 133: 165–177.
19. Lan, J., Y. Yao, Y. Deng, H. Chen, G. Lu, W. Wang, L. Bao, W. Deng, Q. Wei, G. F. Gao, et al. 2015. Recombinant receptor binding domain protein induces partial protective immunity in rhesus macaques against Middle East respiratory syndrome coronavirus challenge. *EBioMedicine* 2: 1438–1446.
20. Lan, J., Y. Deng, H. Chen, G. Lu, W. Wang, X. Guo, Z. Lu, G. F. Gao, and W. Tan. 2014. Tailoring subunit vaccine immunity with adjuvant combinations and delivery routes using the Middle East respiratory coronavirus (MERS-CoV) receptor-binding domain as an antigen. *PLoS One* 9: e112602.
21. Volz, A., A. Kupke, F. Song, S. Jany, R. Fux, H. Shams-Eldin, J. Schmidt, C. Becker, M. Eickmann, S. Becker, and G. Sutter. 2015. Protective efficacy of recombinant modified vaccinia virus ankara delivering Middle East respiratory syndrome coronavirus spike glycoprotein. *J. Virol.* 89: 8651–8656.
22. Guo, X., Y. Deng, H. Chen, J. Lan, W. Wang, X. Zou, T. Hung, Z. Lu, and W. Tan. 2015. Systemic and mucosal immunity in mice elicited by a single immunization with human adenovirus type 5 or 41 vector-based vaccines carrying the spike protein of Middle East respiratory syndrome coronavirus. *Immunology* 145: 476–484.
23. Sun, L., Y. Zhang, B. Zhao, M. Deng, J. Liu, X. Li, J. Hou, M. Gui, S. Zhang, X. Li, et al. 2014. A new unconventional HLA-A2-restricted epitope from HBV core protein elicits antiviral cytotoxic T lymphocytes. *Protein Cell* 5: 317–327.
24. Zhao, J., K. Li, C. Wohlford-Lenane, S. S. Agnihotram, C. Felt, J. Zhao, M. J. Gale, Jr., R. S. Baric, L. Enjuanes, T. Gallagher, et al. 2014. Rapid generation of a mouse model for Middle East respiratory syndrome. *Proc. Natl. Acad. Sci. USA* 111: 4970–4975.
25. Liu, J., Y. Sun, J. Qi, F. Chu, H. Wu, F. Gao, T. Li, J. Yan, and G. F. Gao. 2010. The membrane protein of severe acute respiratory syndrome coronavirus acts as a dominant immunogen revealed by a clustering region of novel functionally and structurally defined cytotoxic T-lymphocyte epitopes. *J. Infect. Dis.* 202: 1171–1180.
26. Liu, J., S. Zhang, S. Tan, Y. Yi, B. Wu, B. Cao, F. Zhu, C. Wang, H. Wang, J. Qi, and G. F. Gao. 2012. Cross-allele cytotoxic T lymphocyte responses against 2009 pandemic H1N1 influenza A virus among HLA-A24 and HLA-A3 supertype-positive individuals. *J. Virol.* 86: 13281–13294.
27. Zhang, S., J. Liu, H. Cheng, S. Tan, J. Qi, J. Yan, and G. F. Gao. 2011. Structural basis of cross-allele presentation by HLA-A*0301 and HLA-A*1101 revealed by two HIV-derived peptide complexes. *Mol. Immunol.* 49: 395–401.
28. Liu, J., B. Wu, S. Zhang, S. Tan, Y. Sun, Z. Chen, Y. Qin, M. Sun, G. Shi, Y. Wu, et al. 2013. Conserved epitopes dominate cross-CD8⁺ T-cell responses against influenza A H1N1 virus among Asian populations. *Eur. J. Immunol.* 43: 2055–2069.
29. Yao, S., J. Liu, J. Qi, R. Chen, N. Zhang, Y. Liu, J. Wang, Y. Wu, G. F. Gao, and C. Xia. 2016. Structural illumination of equine MHC class I molecules highlights unconventional epitope presentation manner that is evolved in equine leukocyte antigen alleles. *J. Immunol.* 196: 1943–1954.
30. Xiao, J., W. Xiang, Y. Chai, J. Haywood, J. Qi, L. Ba, P. Qi, M. Wang, J. Liu, and G. F. Gao. 2016. Diversified anchoring features the peptide presentation of DLA-88*50801: first structural insight into domestic dog MHC class I. *J. Immunol.* 197: 2306–2315.
31. Brünger, A. T., P. D. Adams, G. M. Clore, W. L. DeLano, P. Gros, R. W. Grosse-Kunstleve, J. S. Jiang, J. Kuszewski, M. Nilges, N. S. Pannu, et al. 1998. Crystallography & NMR system: a new software suite for macromolecular structure determination. *Acta Crystallogr. D Biol. Crystallogr.* 54: 905–921.
32. Emsley, P., B. Lohkamp, W. G. Scott, and K. Cowtan. 2010. Features and development of *Coot*. *Acta Crystallogr. D Biol. Crystallogr.* 66: 486–501.
33. Collaborative Computational Project, Number 4. 1994. The CCP4 suite: programs for protein crystallography. *Acta Crystallogr. D Biol. Crystallogr.* 50: 760–763.
34. Laskowski, R. A., M. W. Macarthur, D. S. Moss, and J. M. Thornton. 1993. PROCHECK: a program to check the stereochemical quality of protein structures. *J. Appl. Cryst.* 26: 283–291.
35. Mitaksov, V., and D. H. Fremont. 2006. Structural definition of the H-2K^d peptide-binding motif. *J. Biol. Chem.* 281: 10618–10625.
36. Samanta, D., G. Mukherjee, U. A. Ramagopal, R. J. Chaparro, S. G. Nathenson, T. P. DiLorenzo, and S. C. Almo. 2011. Structural and functional characterization of a single-chain peptide-MHC molecule that modulates both naive and activated CD8⁺ T cells. *Proc. Natl. Acad. Sci. USA* 108: 13682–13687.
37. Motozono, C., J. A. Pearson, E. De Leenheer, P. J. Rizkallah, K. Beck, A. Trimby, A. K. Sewell, F. S. Wong, and D. K. Cole. 2015. Distortion of the major histocompatibility complex class I binding groove to accommodate an insulin-derived 10-mer peptide. *J. Biol. Chem.* 290: 18924–18933.
38. Chen, J., and K. Subbarao. 2007. The immunobiology of SARS. *Annu. Rev. Immunol.* 25: 443–472.
39. Liu, J., S. Zhang, S. Tan, B. Zheng, and G. F. Gao. 2011. Revival of the identification of cytotoxic T-lymphocyte epitopes for immunological diagnosis, therapy and vaccine development. *Exp. Biol. Med. (Maywood)* 236: 253–267.
40. Li, C. K., H. Wu, H. Yan, S. Ma, L. Wang, M. Zhang, X. Tang, N. J. Temperton, R. A. Weiss, J. M. Brenchley, et al. 2008. T cell responses to whole SARS coronavirus in humans. *J. Immunol.* 181: 5490–5500.
41. Zhou, M., D. Xu, X. Li, H. Li, M. Shan, J. Tang, M. Wang, F. S. Wang, X. Zhu, H. Tao, et al. 2006. Screening and identification of severe acute respiratory syndrome-associated coronavirus-specific CTL epitopes. *J. Immunol.* 177: 2138–2145.
42. Wang, B., H. Chen, X. Jiang, M. Zhang, T. Wan, N. Li, X. Zhou, Y. Wu, F. Yang, Y. Yu, et al. 2004. Identification of an HLA-A*0201-restricted CD8⁺ T-cell epitope SSp-1 of SARS-CoV spike protein. *Blood* 104: 200–206.
43. Wang, Y. D., W. Y. Sin, G. B. Xu, H. H. Yang, T. Y. Wong, X. W. Pang, X. Y. He, H. G. Zhang, J. N. Ng, C. S. Cheng, et al. 2004. T-cell epitopes in severe acute respiratory syndrome (SARS) coronavirus spike protein elicit a specific T-cell immune response in patients who recover from SARS. *J. Virol.* 78: 5612–5618.
44. Zhao, J., J. Zhao, and S. Perlman. 2010. T cell responses are required for protection from clinical disease and for virus clearance in severe acute respiratory syndrome coronavirus-infected mice. *J. Virol.* 84: 9318–9325.
45. Zhao, J., Q. Huang, W. Wang, Y. Zhang, P. Lv, and X. M. Gao. 2007. Identification and characterization of dominant helper T-cell epitopes in the nucleocapsid protein of severe acute respiratory syndrome coronavirus. *J. Virol.* 81: 6079–6088.
46. Zhi, Y., G. P. Kobinger, H. Jordan, K. Suchma, S. R. Weiss, H. Shen, G. Schumer, G. Gao, J. L. Boyer, R. G. Crystal, and J. M. Wilson. 2005. Identification of murine CD8 T cell epitopes in codon-optimized SARS-associated coronavirus spike protein. *Virology* 335: 34–45.
47. Liu, J., J. Qi, F. Gao, J. Yan, and G. F. Gao. 2011. Functional and structural definition of a clustering region of HLA-A2-restricted cytotoxic T lymphocyte epitopes. *Sci. Technol. Rev.* 29: 9–27.
48. Zhang, S., R. K. Bakshi, P. V. Suneetha, P. Fytilli, D. A. Antunes, G. F. Vieira, R. Jacobs, C. S. Klade, M. P. Manns, A. R. Kraft, et al. 2015. Frequency, private specificity, and cross-reactivity of preexisting hepatitis C virus (HCV)-specific CD8⁺ T cells in HCV-seronegative individuals: implications for vaccine responses. *J. Virol.* 89: 8304–8317.
49. Valkenburg, S. A., S. Gras, C. Guillonnet, L. A. Hatton, N. A. Bird, K. A. Twist, H. Halim, D. C. Jackson, A. W. Purcell, S. J. Turner, et al. 2013. Preemptive priming readily overcomes structure-based mechanisms of virus escape. *Proc. Natl. Acad. Sci. USA* 110: 5570–5575.
50. Valkenburg, S. A., S. Gras, C. Guillonnet, N. L. La Gruta, P. G. Thomas, A. W. Purcell, J. Rossjohn, P. C. Doherty, S. J. Turner, and K. Kedzierska. 2010. Protective efficacy of cross-reactive CD8⁺ T cells recognising mutant viral epitopes depends on peptide-MHC-I structural interactions and T cell activation threshold. *PLoS Pathog.* 6: e1001039.
51. Li, X., J. Liu, J. Qi, F. Gao, Q. Li, X. Li, N. Zhang, C. Xia, and G. F. Gao. 2011. Two distinct conformations of a rinderpest virus epitope presented by bovine major histocompatibility complex class I N*01801: a host strategy to present featured peptides. *J. Virol.* 85: 6038–6048.